Journal of ELECTRONIC MATERIALS, Vol. 50, No. 4, 2021
https://doi.org/10.1007/s11664-020-08500-4

ASIAN CONSORTIUM ACCMS–INTERNATIONAL CONFERENCE ICMG 2020

Enhanced Magnetoelectric Effects in Self-Assembled Hemispherical Close-Packed $CoFe_2O_3$-$Pb(Zr_{0.52}Ti_{0.48})O_3$ Thin Film

SRIDEVI MEENACHISUNDARAM,[1,4] NAOKI WAKIYA,[1,2,3] CHELLAMUTHU MUTHAMIZHCHELVAN,[4,6,7] PARTHASARATHI GANGOPADHYAY,[5] NAONORI SAKAMOTO,[2,3] and SURUTTAIYUDAIYAR PONNUSAMY[4]

1.—Graduate School of Science and Technology, Shizuoka University, Hamamatsu 432–8561, Japan. 2.—Department of Electronics and Materials Science, Shizuoka University, Hamamatsu 432–8561, Japan. 3.—Research Institute of Electronics, Shizuoka University, Hamamatsu 432–8561, Japan. 4.—Department of Physics and Nanotechnology, SRM Institute of Science and Technology, Chennai 603–203, India. 5.—Indira Gandhi Centre for Atomic Research, Kalpakkam, Tamil Nadu 603–102, India. 6.—e-mail: selvan.cm@srmuniv.ac.in. 7.—e-mail: selvancm@gmail.com

With their promising enhanced magnetoelectric (ME) effects and multifunctional properties, 2D ME materials are garnering considerable research interest. However, experimental studies regarding ME effects are sparse. In order to enhance ME properties, it may be important to develop a strategy to prepare ordered ME thin film materials on suitable substrates. Materials ought to possess high surface area and less area of contact with the substrate. We investigate ME thin films consisting of $CoFe_2O_4$ (CFO)/$Pb(Zr_{0.52}Ti_{0.48})O_3$ (PZT)/$LaNiO_3$·(LNO) on a Pt/Ti/SiO_2/Si substrate that were prepared using a radio-frequency magnetron sputtering technique. The method helps to relax the in-plane constraint force and enhances the coexistence of the ferromagnetic and ferroelectric phases at the interface of the materials. Interestingly, the freestanding hemispherical ME thin films exhibited huge changes in magnetic field-induced polarization. Compared with planar CFO/PZT thin films of similar dimensions, the measured polarization was more than twice as large in the freestanding hemispherical ME thin films. This facile physico-chemical technique for preparing highly efficient, hierarchically ordered micro/nano-magnetoelectric thin films may be used for the fabrication of miniaturized devices.

Key words: Freestanding thin films, ME effect, polarization, clamping force

INTRODUCTION

Magnetoelectric (ME) composite thin films, due to their multifunctional properties and promising enhanced ME effects, have garnered ever-increasing interest over the past few decades.[1,2] The coupling interaction between the ferromagnetic and ferroelectric layers is developed in this ME material. This ME coupling interaction has possible applications in multilevel recording memory[3,4] and low-power-consumption magnetic memory devices.[5,6] Thin films prepared under the same deposition conditions reveal improved properties just by changing the structure, and thus such thin

(Received March 20, 2020; accepted September 19, 2020; published online October 21, 2020)

films are expected to be applied to various fields and attract much attention.[7] Multifunctional devices like ME random access memory[8] and ME microsensors[9] utilize the coexistence of polarization and magnetization. The strain generated by the magnetostrictive or piezostrictive layer in ME thin films is called the direct or converse ME effect, respectively.[10] There are two general strategies for deriving ME coupling: strain-mediated ME coupling[10–12] and coupling produced directly without the application of strain.[13,14] In the case of single-phase ME materials, coupling is produced directly by the ME parameters without applying any strain, so it is possible for the ME effect to be deteriorated by any one parameter even though the others are strong. But in the ME composite thin films, the composite design affects the interaction between the ferroelectric layer and magnetostrictive layer.

As reported earlier, the ME effect is limited in two-dimensional (2D) ferroelectric-magnetostrictive thin films because of the in-plane constraint force.[15–18] This clamping force on substrate-supported thin film can reduce the ME effect. Once the in-plane constraint force is relaxed in the ME films, strain-mediated interaction between the ferroelectric and magnetostrictive layers can occur. Compared to one-dimensional vertical heterostructures, 2D thin films show weak interaction between the ferroelectric and magnetostrictive layers.[19–21] Growth of buffer layers [i.e., $LaNiO_3$ (LNO) layer[22–24] between the substrate and composite films has an important dual role: while enhancing the strain-mediated ME effect, it relaxes the clamping force constraints from the substrates. Zhang et al. found very weak electrical properties in 2D layered composite films.[1] The in-plane constraint from the substrate, as explained, affected the ME coupling in the 2D layered films. To relax this constraint effect, buffer layers are grown between the substrate and composite films.[25] Haeni et al. developed a new substrate with critical thickness to improve the growth of strained films. This can enhance the growth of the film due to tensile or compressive strain, depending upon the choice of material.[26] Erenstein et al. confirmed that for single-phase materials, the changes in polarization were not permanent, as they occurred only at low temperatures.[16] Wang et al. observed that two constituent phases combined at the atomic level could reduce the interface losses rather than the composites made by co-sintering and adhesive bonding methods.[10] Zhang et al. determined that the compressive strain between $CoFe_2O_4$ (CFO) and $SrTiO_3$ was reduced with increasing thickness of CFO film, indicating that the coupling was highly dependent on the film thickness.[27] These studies were all aimed at enhancing the coupling in ME materials.

Therefore, in this study, we aimed to study the enhancement of the coupling mechanism in freestanding hemispherical ME thin films. When the freestanding structure was compared with normal thin film of similar dimensions (i.e., flat film), the freestanding hemispherical thin film exhibited enhanced ME properties. As demonstrated in this report, hollow spaces inside the freestanding hemispherical thin film relax the in-plane constraint force because of less contact area with the substrate, and enhance the coexistence of the ferromagnetic and ferroelectric phases at the interface of the CFO/$Pb(Zr_{0.52}Ti_{0.48})O_3$ (PZT) materials.

Fabrication of ME Thin Film

PMMA monolayer colloidal crystals (MCCs) with a close-packed structure (CPS) were fabricated on cleaned Pt/Ti/SiO_2/Si substrates by a dip-coating technique with a dipping speed of 1 mm/s. The substrates (1 cm^2 dimension) were cleaned ultrasonically in acetone for 10 min and rinsed with water for 2 min. No additional treatment such as RCA cleaning was carried out, and Si with natural oxide was used as substrate. Initially, MCC solution containing 1 μm PMMA was prepared, and the stoichiometric targets of CFO, PZT, and LNO were prepared through a solid-state reaction process, as described previously.[23] In this approach, we initially fabricated freestanding hemispherical $LaNiO_3$ arrays by the self-assembly of monolayers, followed by radio-frequency (RF) sputtering. The steps involved in fabricating the close-packed freestanding hemispherical ME thin film on the substrate have been explained elsewhere.[23] In our previous studies, we compared the magnetoelectric properties of flat and freestanding thin films prepared using a pulsed laser deposition (PLD) method. LNO was a bottom electrode, and NiO was used as a seed layer. In the present study, for homogeneous deposition of CFO/PZT/LNO multiferroic thin films, RF magnetron sputtering was used. Here, LNO was used as both the bottom electrode and seed layer. First, a monolayer PMMA template was prepared as hierarchically close-packed arrays on the substrate. Subsequently, a thin layer of LNO film was deposited at room temperature on the PMMA template using RF magnetron sputtering. To incinerate this PMMA template and crystallize the LNO as the buffer layer and bottom electrode, an LNO layer was again deposited at 450°C. The LNO thin film inherited the freestanding hemispherical shell structure and hollow space from the spherical template upon thermal removal of the template. This LNO thin film was used as a buffer layer to enhance the crystallinity of the film and as the bottom electrode. Subsequently, PZT as ferroelectric thin film and CFO as ferromagnetic thin film were deposited on the freestanding buffer layer thin film

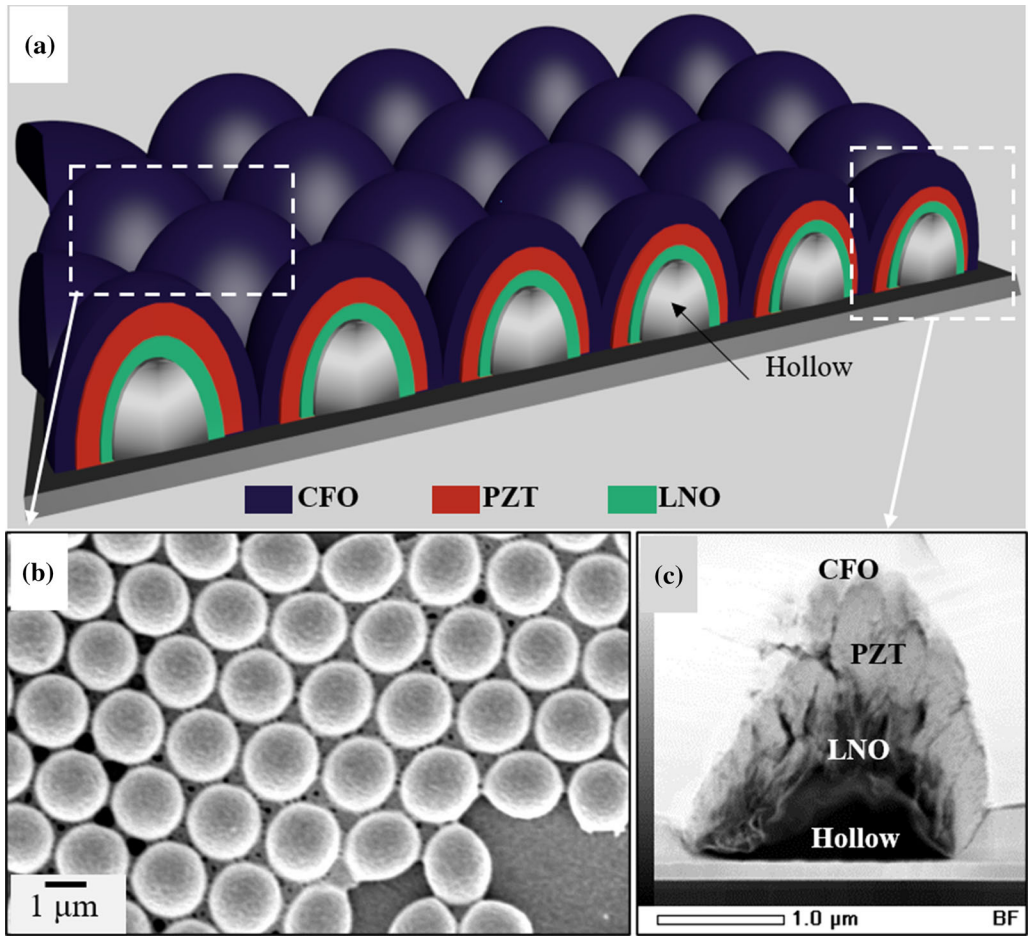

Fig. 1. Freestanding hemispherical CFO/PZT/LNO thin film on Pt/Ti/SiO_2/Si. (a) The corresponding illustrated image, (b) top view of the SEM image, and (c) the cross-sectional STEM image of the single shell.

Table I. Parameters and conditions for CFO/PZT/LNO ME thin film deposition using the RF magnetron sputtering technique

Material layers	Temperature (°C)	O_2 pressure (Pa)	Film composition (mol. ratio)	Film thickness (nm)
1 - LNO	RT	2	$LaNiO_3$	100
2 - LNO	450	2	$LaNiO_3$	200
3 - PZT	550	3	$Pb_{1.1}(Zr_{0.52}Ti_{0.48})O_3$	410
4 - CFO	700	2	$Co_{0.95}Fe_{2.05}O_4$	130

by a sputtering technique without breaking the vacuum. We successfully fabricated the CFO/PZT/LNO ME thin film with a 2D array of a close-packed structure on the bottom electrode by a physicochemical approach (see Fig. 1a). We call this thin film freestanding hemispherical thin film. Figure 1b and c shows corresponding SEM images and cross-sectional view of the STEM image of the single shell. CFO/PZT/LNO thin films were also deposited using the same conditions on the substrate (called the flat film) to compare the properties of the flat film with the freestanding hemispherical thin film.

The composition of the ME thin film was determined using x-ray fluorescence spectroscopy (XRF). The sputtering parameters chosen for the deposition of the ME thin film were as follows: RF power 150 W/cm^2, target–substrate distance of 20 mm and Ar:O_2 ratio = 8:2. The film composition, deposition conditions and thickness of the freestanding hemispherical ME thin film are provided in Table I. The sputtering technique was utilized to deposit Pt metal dots ($\sim$ 100 μm diameters) on the ME thin film. These Pt microstructures served as the top electrode.

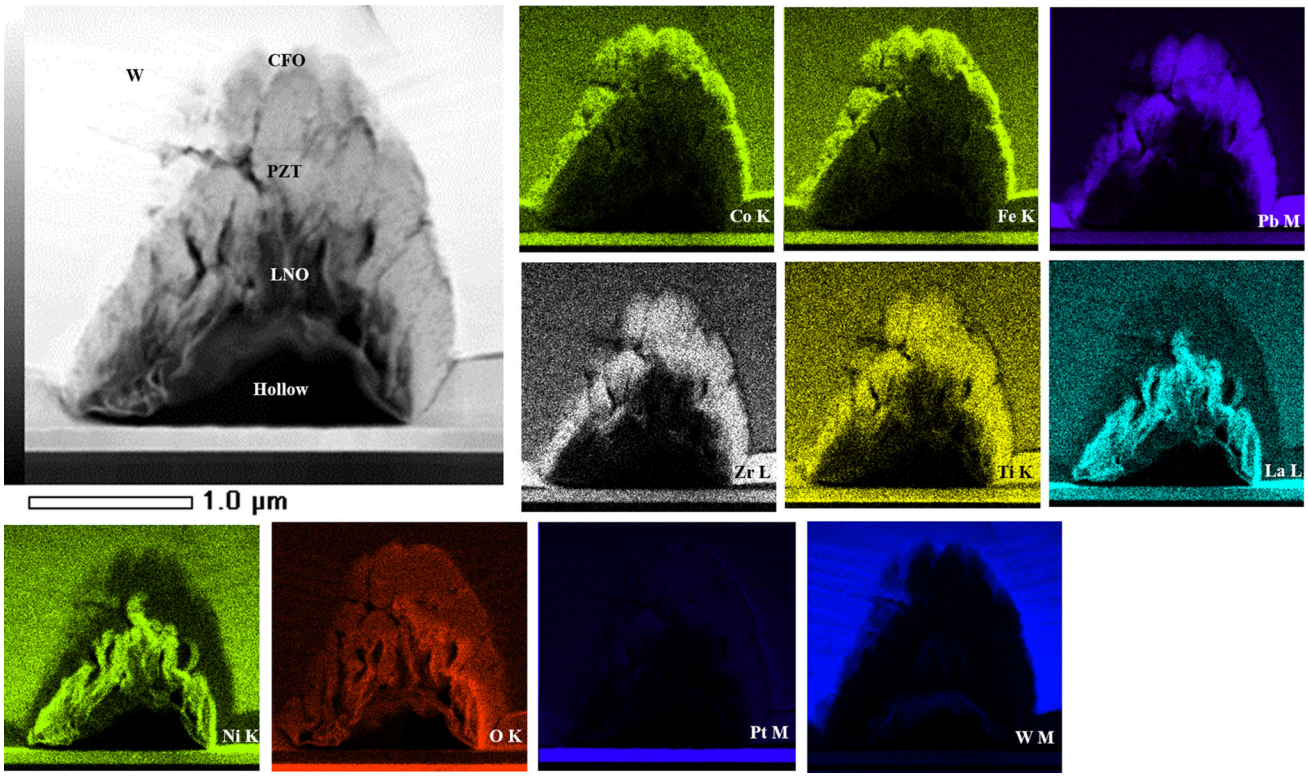

Fig. 2. Bright-field STEM image of the cross-section of a single shell CFO/PZT/LNO thin film and STEM-EDS mapping of each element for the single freestanding hemispherical CFO/PZT/LNO shell.

Material Characterization

The crystal structure of the ME thin film was examined using a D8 Advance x-ray diffractometer (Bruker AXS). The thickness and composition of the films were estimated using x-ray fluorescence spectroscopy (XRF, MiniPal, PANalytical B.V., Netherlands). The surface morphology images were recorded using a scanning electron microscope (SEM, JSM-5010LV; JEOL). A scanning transmission electron microscope (STEM, JEM-2100F; JEOL), equipped with an energy-dispersive x-ray spectrometer (EDS), was utilized for cross-sectional analysis of each layer of the freestanding hemispherical shell thin film. The *M–H* hysteresis loop and *P–H* loop were measured using a vibrating-sample magnetometer (VSM, Rigaku BHV-35) and a ferroelectric measurement setup (FC-E; TOYO Corporation), respectively.

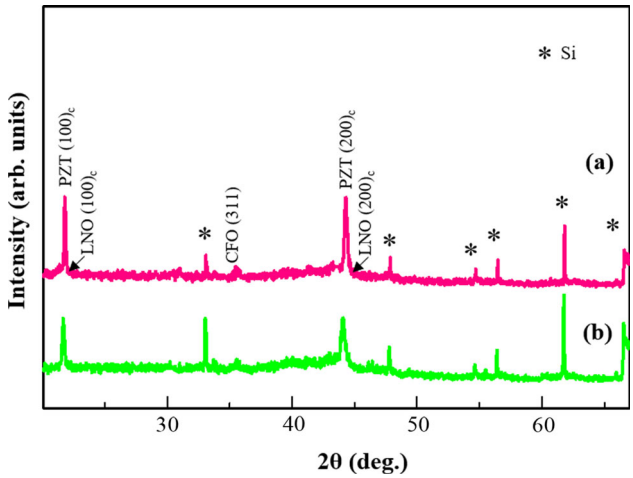

Fig. 3. X-ray diffraction pattern of (a) flat and (b) freestanding hemispherical CFO/PZT/LNO thin film.

RESULTS AND DISCUSSION

Microscopic Analysis of Close-Packed Freestanding Hemispherical ME Thin Film

Figure 2 shows the cross-sectional STEM image of freestanding hemispherical single ME shell on the substrate, which was acquired with bright-field imaging (see Fig. 2). Freestanding growth of the thin film, composition and morphology of the single ME shell were confirmed by EDS mapping. Based on the EDS analysis, the arrangement of the LNO (La L, Ni K, O K) thin film followed by PZT (Pb M, Zr L, Ti K, O K) and CFO (Co K, Fe K, O K) thin films on the hollow space was confirmed. The interior of the ME thin film had a hollow space corresponding to the evaporation of the PMMA template. The hollow space inside the ME thin film in each EDS image confirmed that no interdiffusion of atoms occurred between the film and substrate. Figure 3 shows the corresponding x-ray diffraction

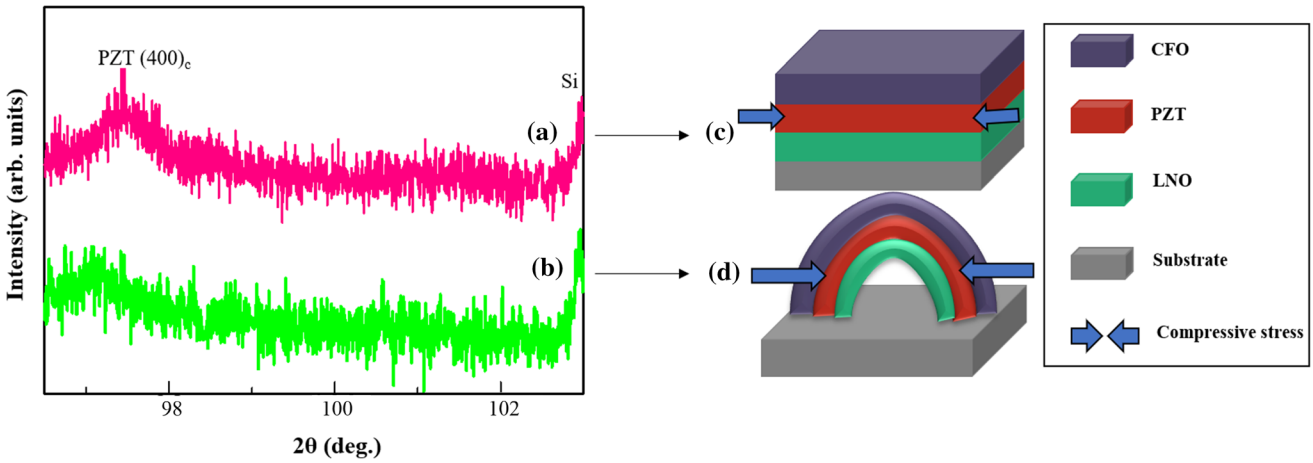

Fig. 4. X-ray diffraction patterns at high 2θ angles for (a) flat and (b) freestanding hemispherical CFO/PZT/LNO thin films. Schematic illustration of stacking for (c) flat and (d) freestanding hemispherical CFO/PZT/LNO thin films.

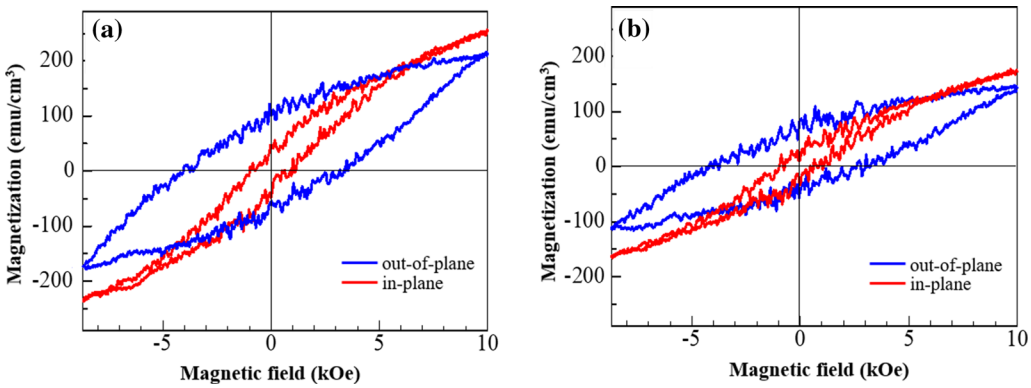

Fig. 5. *M–H* curves for (a) flat thin films and (b) freestanding hemispherical CFO/PZT/LNO thin films.

(XRD) pattern confirming the presence of perovskite and spinel structures. The XRD results thus suggest the successful synthesis of the preferentially oriented perovskite thin film on the buffer layer.

Increased Compressive Strain in Freestanding Hemispherical ME Thin Film

Figure 4 shows the high-angle 2θ x-ray diffraction (XRD) pattern for the flat and freestanding hemispherical ME thin films. The diffraction peak positions (2θ) for the freestanding and flat thin films were found to be 97.05° and 97.45°, respectively. As reported earlier, a pseudo cubic (rhombohedral) $(400)_c$ symmetry peak for the PZT bulk appears at $2\theta = 98.0°$.[28] The results shown in Fig. 4a and b are in good agreement with the reported results, and confirm that the PZT layer grown on the ME thin film has pseudo cubic $(400)_c$ symmetry for both thin films. Interestingly, as shown in Fig. 4, the diffraction peak positions for $(400)_c$ differ between the two films. This result may be explained by the following three possibilities: (1) difference in chemical composition, (2) misalignment of XRD and (3) different levels of strain. However, the first two possibilities may be excluded. We measured the composition of the flat and freestanding hemispherical thin films by XRF, which confirmed that there were no compositional deviations between these two thin films. The possibility of misalignment of XRD is also excluded, because we always carried out the calibration of the 2θ position using the peak position of Si (400). Therefore, we may conclude that the peak position shift toward the low-angle side in the freestanding hemispherical thin film is caused by the compressive strain. The strain generated is greater in the freestanding hemispherical thin film than in the flat thin film due to the higher thermal expansion coefficients of LNO than PZT.[23,24]

Magnetoelectric Studies of ME Thin Films

Figure 5 shows the magnetization (M)–magnetic field (H) curves for the CFO layer measured at room temperature by applying a magnetic field up to 10 kOe. The in-plane saturation magnetization of the freestanding hemispherical film and the flat film ($\sim$ 200 emu/cm^3) is smaller than that of the bulk

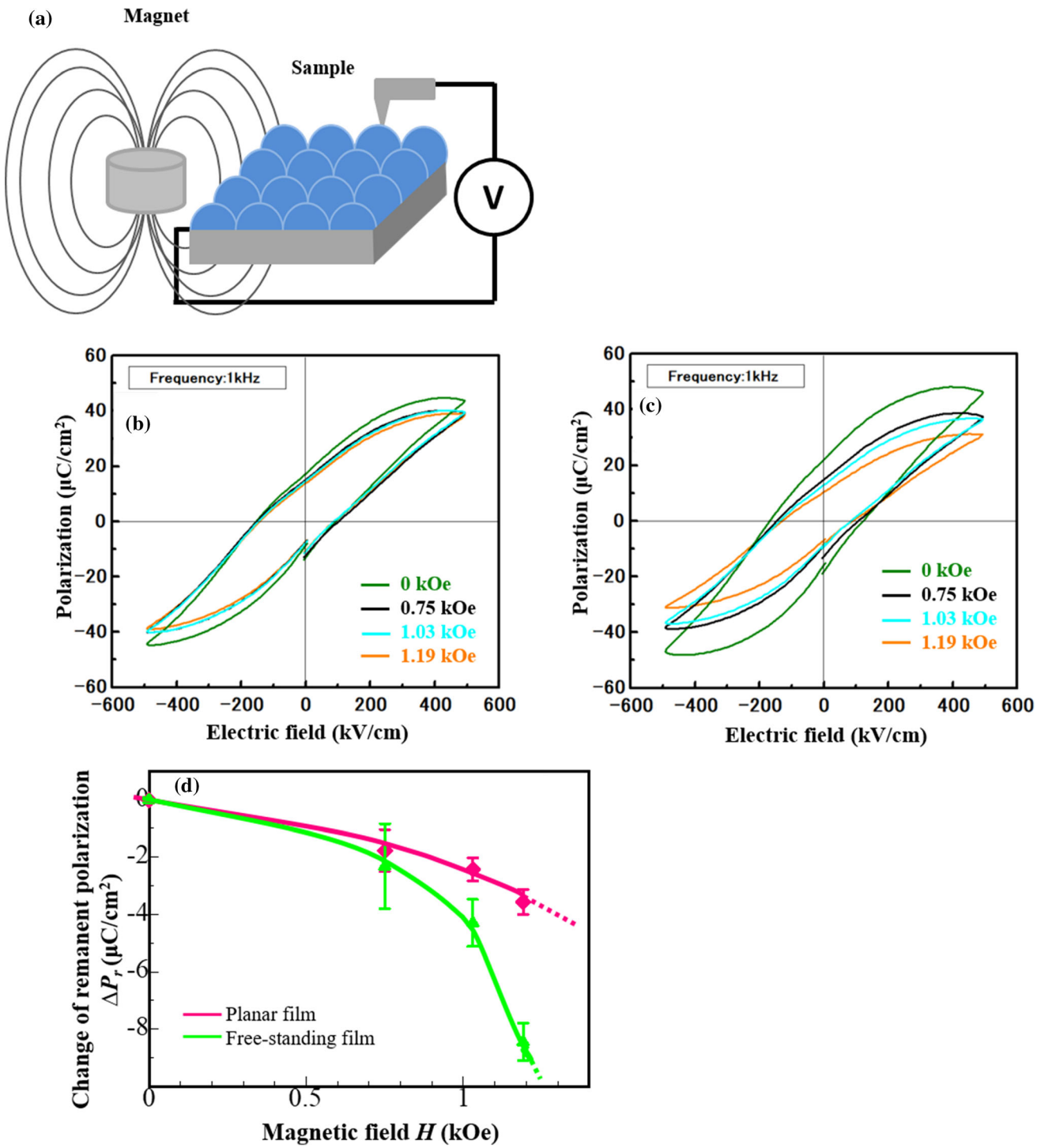

Fig. 6. (a) Schematic drawing of the application of external magnetic field perpendicular to the substrate. (b) and (c) Change in *P*–*E* curves with the applied external magnetic field for flat and freestanding hemispherical CFO/PZT/LNO thin films, respectively. (d) Change in P_r with the applied external magnetic field for flat and freestanding hemispherical CFO/PZT/LNO thin films.

CFO ($\sim$ 425 emu/cm^3).[29,30] In this work, we define the in-plane and out-of-plane magnetic measurements as the direction of the Si substrate. This definition is applied for both the flat and freestanding hemispherical thin films. Though each hemispherical thin film has a curved surface, the films are arranged in a 2D array. This is because the thin film was prepared using 2D close-packed monodisperse PMMA particles. Therefore, from the point of the aggregate, the hemispherical thin film can be regarded as a porous thin film. The results shown in Fig. 5a and b suggest perpendicular magnetic

anisotropy for both planar and freestanding thin films. Because CFO is a well-known perpendicular magnetic anisotropy material, the perpendicular magnetic anisotropy shown in Fig. 5a and b would derive from the nature of CFO.

A comparison of Fig. 5a and b suggests that the shape of the *M–H* curve is similar. Therefore, it is considered that the strain does not give an apparent difference in magnetic anisotropy. The recorded hysteresis curves also display highly anisotropic magnetic behaviors.

An AFM system (SPI3800N with SPA-400 scanner, Hitachi High-Tech Corp., Japan) was used for the ferroelectric measurement using a conductive probe (SI-DF20-R, Hitachi High-Tech Corp., Japan; stiffness: 15 N/m). During the ferroelectric measurement, there was no mechanical stress applied from the probe to the sample that could break down the shell structure. The scanner automatically compensates the z-axis motion of the sample through a feedback signal mechanism sensed by the probe. The authors consider that the shell structure has the mechanical stability to withstand ferroelectric measurements without breaking down. A schematic illustration of the measurement of the ferroelectric loops of the flat and the freestanding hemispherical thin films by applying the magnetic field is shown in Fig. 6a. The change in polarization value by applying the magnetic field indicates that it is feasible to polarize ferroelectric domains at a frequency of 1 kHz (see Fig. 6b). The maximum change in remanent polarization value for the flat and the freestanding hemispherical film is 19 and 22.5 $\mu C/cm^2$, respectively, in the absence of the magnetic field, and it starts to decrease up to an applied magnetic field of 1.19 kOe (Fig. 6c and d). Measurements suggest that the presence of ME coupling is through two-order parameters in both films. Figure 6d shows the change in the remanent polarization curve corresponding to the applied magnetic field. The pink line indicates the remanent polarization curve for the planar ME thin film, and the green line represents the freestanding hemispherical ME thin film. The inherent nature of the ME coupling in the ME films is more complex than that of bulk ME composites because of complicated residual strain status in the films.[1] In order to enhance the ME coupling in ME thin films, we fabricated the freestanding hemispherical structure to reduce the effect of clamping force from the substrate. In both cases of ME thin films, a change in remanent polarization decreased almost linearly after applying the magnetic field of 0.75 kOe. In the case of freestanding hemispherical thin film, the decrease in remanent polarization value was more than twice (8.5 $\mu C/cm^2$) that of the flat film (3.56 $\mu C/cm^2$), and the change in remanent polarization decreases linearly with the increase in the magnetic field owing to the relaxation of the substrate constraint force.

CONCLUSION

We fabricated ME composite thin films (CFO/PZT/LNO) with a flat structure and a freestanding hemispherical structure. These films were prepared using self-assembly and RF sputtering techniques, and their ME characteristics were evaluated. Even though the magnetostriction effect of the magnetic layer was sufficient to induce polarization on the ferroelectric layer in both films, the freestanding hemispherical thin film exhibited the larger ME effect. This is because of the relaxation of the restrictive force from the substrate, enhancing the ME coupling at the interface of spinel CFO and perovskite PZT materials.

CONFLICT OF INTEREST

The authors declare that they have no conflict of interest.

REFERENCES

1. H.R. Zhang, K. Kalantari, D.M. Marincel, S. Trolier-Mc Kinstry, I. MacLaren, Q.M. Ramasse, W.M. Rainforth, and I.M. Reaney, *Thin Solid Films* 616, 767 (2016).
2. P. Mandal, M.J. Pitcher, J. Alaria, H. Niu, P. Borisov, P. Stamenov, J.B. Claridge, and M.J. Rosseinsky, *Nature* 525, 363 (2015).
3. E.Y. Tsymbal and H. Kohlstedt, *Science* 313, 181 (2006).
4. M. Gajek, M. Bibes, S. Fusil, K. Bouzehouane, J. Fontcuberta, A. Barthélémy, and A. Fert, *Nat. Mater.* 6, 296 (2007).
5. S. Dussan, A. Kumar, J.F. Scott, S. Priya, and R.S. Katiyar, *Appl. Phys. Lett.* 97, 252902 (2010).
6. S. Dussan, A. Kumar, R.S. Katiyar, S. Priya, and J.F. Scott, *J. Phys. Condens. Matter* 23, 202203 (2011).
7. R. Usami, N. Sakamoto, K. Shinozaki, H. Suzuki, and N. Wakiya, *Sci. Technol. Adv. Mater.* 12, 034406 (2011).
8. M. Bibes and A. Barthelemy, *Nat. Mater.* 7, 425 (2008).
9. S. Dussan, A. Kumar, J.F. Scott, and R.S. Katiyar, *Appl. Phys. Lett.* 96, 072904 (2010).
10. Y. Wang, J. Hu, Y. Lin, and C.W. Nan, *NPG Asia Mater.* 2, 61 (2010).
11. J. Ma, J. Hu, Z. Li, and C.W. Nan, *Adv. Mater.* 23, 1062 (2011).
12. W. Eerenstein, F.D. Morrison, J. Dho, M.G. Blamire, J.F. Scott, and N.D. Mathur, *Science* 419, 1203a (2005).
13. Y.H. Chu, L.W. Martin, M.B. Holcomb, and R. Ramesh, *Mater. Today* 10, 16 (2007).
14. Z. Li, Y. Gao, B. Yang, Y. Lin, R. Yu, and C.W. Nan, *J. Am. Ceram. Soc.* 94, 1060 (2011).
15. Z. Li, Y. Wang, Y. Lin, and C.W. Nan, *Phys. Rev. B* 79, 180406 (2009).
16. W. Eerenstein, N.D. Mathur, and J.F. Scott, *Nature* 442, 759 (2006).
17. W.F. Brown, R.M. Hornreigh, and S. Shtrikman, *Phys. Rev.* 168, 178 (1968).
18. H. Zhao, X. Peng, L. Zhang, J. Chen, W. Yan, and X. Xing, *Appl. Phys. Lett.* 103, 082904 (2013).
19. M.I. Bichurin and V.M. Petrov, *Phys. Rev. B* 68, 054402 (2003).
20. F. Zavaliche, H. Zheng, L. Mohaddes-Ardabili, S.Y. Yang, Q. Zhan, P. Shafer, E. Reilly, R. Chopdekar, Y. Jia, P. Wright, D.G. Schlom, Y. Suzuki, and R. Ramesh, *Nano Lett.* 5, 1793 (2005).
21. F. Zavaliche, T. Zhao, H. Zheng, F. Straub, M.P. Cruz, P.L. Yang, D. Hao, and R. Ramesh, *Nano Lett.* 7, 1586 (2007).
22. M. Zhu, X. Dong, Y. Chen, F. Xue, J. Lian, L. Xiao, G. Ding, and G. Wang, *Ceram. Int.* 42, 13925 (2016).
23. S. Meenachisundaram, T. Kawaguchi, R. Usami, N. Sakamoto, K. Shinozaki, C. Muthamizhchelvan, S. Ponnusamy, H. Suzuki, and N. Wakiya, *J. Alloys Compd.* 730, 369 (2018).

24. T. Ohno, H. Yanagida, K. Maekawa, T. Arai, N. Sakamoto, N. Wakiya, H. Suzuki, S. Satoh, and T. Matsuda, *Thin Solid Films* 585, 91 (2015).
25. H. Zheng, J. Wang, S.E. Lofland, Z. Ma, L. Mohaddes-Ardabili, T. Zhao, L. Salamanca-Riba, S.R. Shinde, S.B. Ogale, F. Bai, D. Viehland, Y. Jia, D.G. Schlom, M. Wuttig, A. Roytburd, and R. Ramesh, *Science* 303, 661 (2004).
26. J.H. Haeni, P. Irvin, W. Chang, R. Uecker, P. Reiche, Y.L. Li, S. Choudhury, W. Tian, M.E. Hawley, B. Craigo, A.K. Tagantsev, X.Q. Pan, S.K. Streiffer, L.Q. Chen, S.W. Kirchoefer, J. Levy, and D.G. Schlom, *Nature* 430, 758 (2004).
27. J.X. Zhang, J.Y. Dai, C.K. Chow, C.L. Sun, V.C. Lo, and H.L.W. Chan, *Appl. Phys. Lett.* 92, 022901 (2008).
28. J. Joseph, T.M. Vimala, V. Sivasubramanian, and V.R.K. Murthy, *J. Mater. Sci.* 35, 1571 (2000).
29. J. Smit, H. P. J. Wijn, and Ferrites, (Wiley, New York, 1959), p. 156.
30. J.P. Zhou, H.C. He, Z. Shi, and C.W. Nan, *J. Appl. Phys.* 88, 013111 (2006).